Structure of the Active Domain of the Herpes Simplex Virus Protein ICP47 in Water/Sodium Dodecyl Sulfate Solution Determined by Nuclear Magnetic Resonance Spectroscopy[†,‡]

Ruth Pfänder, Lars Neumann, Markus Zweckstetter, Christoph Seger, Tad A. Holak,* and Robert Tampé*[,§]

Max-Planck-Institut für Biochemie, D-82152 Martinsried, Germany

Received April 28, 1999; Revised Manuscript Received July 30, 1999

ABSTRACT: ICP47 encoded by herpes simplex virus (HSV) is a key factor in the evasion of cellular immune response against HSV-infected cells. By specific inhibition of the transporter associated with antigen processing (TAP), ICP47 prevents peptide transport into the endoplasmic reticulum and subsequent loading of major histocompatibility complex (MHC) class I molecules. Amino acid residues 3−34 have been identified as the active domain. This domain appeared to be unstructured in aqueous solution, whereas after binding to membranes an α-helical conformation was observed. Here, we have analyzed the structure of ICP47(2−34) in a lipidlike environment by nuclear magnetic resonance (NMR) spectroscopy. In micellar solution of deuterated sodium dodecyl sulfate, the viral TAP inhibitor adopts an ordered structure. There are two helical regions extending from residues 4 to 15 and from residues 22 to 32. Arg-16 is found on the C-terminus of the first helix, and Gly-33 serves as a terminator of the second helix. A loop between residues 17 and 21 is also evident in the structure. The relative orientation of the helices toward each other, however, could not be determined due to the paucity of NOEs from residues 18−21.

Due to our daily encounter with a vast number of pathogens, evolution equipped us with an adaptive immune system. The major histocompatibility complex (MHC)[1] class I-mediated immunity is mainly responsible for the control of virus-infected cells. Fragments derived from viral proteins are translocated into the endoplasmic reticulum by the transporter associated with antigen processing (TAP). These peptides are loaded onto MHC class I molecules by the assistance of various chaperones. Stable MHC complexes traffic to the cell surface where their cargo is monitored by cytotoxic T-lymphocytes, which eventually initiate lysis (for reviews, see ref *1*). Under this selection pressure, persistent viruses evolved strategies to block the class I antigen presentation pathway in order to escape immune surveillance. Proteins encoded by large DNA and retroviruses in particular have been identified to interfere with the host immune system (for review, see ref *2*).

By blocking peptide supply to MHC class I molecules, the herpes simplex virus protein ICP47 downregulates surface expression of MHC class I molecules in human fibroblasts (*3*, *4*). ICP47 inhibits TAP-dependent translocation of antigenic peptide into the ER (*5*, *6*). High-affinity binding to TAP (K_d = 50 nM) enables the viral inhibitor to compete with peptides for the peptide binding site of human TAP and to block thereby the initial step of peptide transport (*7*, *8*). The ICP47-TAP interaction is highly species-specific, since the viral protein shows a more than 100-fold higher affinity for human than for murine TAP (*7*, *8*). It has been further suggested that binding of ICP47 results in a conformational change of peptide transporter, which might also block TAP function (*9*).

In addition to its exclusive function, ICP47 exhibits an unique primary and secondary structure. Apart from the ICP47 homologue of HSV-2, no related sequences were found in the sequence database. The active domain of ICP47 has recently been mapped (*10*, *11*). The region covering amino acids 3−34 was found to be as active as the full-length protein (*11*). Circular dichroism and NMR spectroscopy revealed that ICP47(2−34) peptide has no secondary structure elements and lacks a uniquely folded conformation in aqueous solution, whereas in the presence of membrane mimetics, such as trifluoroethanol, sodium dodecyl sulfate, or lipid membranes an α-helical structure is induced (*12*). Further evidence for a specific interaction of ICP47 with membranes was obtained by tryptophan fluorescence spectroscopy (*12*) and fluorescence quenching experiments (L.N.

[†] This work was supported by grants (SFB266) from the Deutsche Forschungsgemeinschaft (DFG).

[‡] The coordinates of the structure have been deposited in the Brookhaven Protein Data Bank (entry name 1qlo).

* Corresponding authors: (R.T.) phone +49-6421-286 5004, fax +49-6421-286 4335, e-mail tampe@mailer.uni-marburg.de; (T.A.H.) phone +49-89-8578-2673, fax +49-89-8578-3777, e-mail holak@biochem.mpg.de.

[§] Present address: Zelluläre Biochemie & Biophysik, Institut für Physiologische Chemie, Philipps-Universität Marburg, Karl-von-Frisch-Strasse 1, D-35043 Marburg, Germany.

[1] Abbreviations: MHC, major histocompatibility complex; ER, endoplasmic reticulum; TAP, transporter associated with antigen processing; HSV, herpes simplex virus; SDS, sodium dodecyl sulfate; NMR, nuclear magnetic resonance; NOE, nuclear Overhauser effect; NOESY, two-dimensional nuclear Overhauser effect spectroscopy; TOCSY (HOHAHA), total correlation spectroscopy (homonuclear Hartmann−Hahn spectroscopy); DQF−COSY, double quantum filtered homonuclear correlated spectroscopy; 2D, two-dimensional; 3D, three-dimensional; D_2O, deuterated water; TPPI, time-proportional phase incrementation; rmsd, root-mean-square difference; rms, root-mean-square; SA, simulated annealing.

10.1021/bi9909647 CCC: $18.00
Published on Web 09/17/1999

and R.T., unpublished data). Here, we first investigated the interaction of ICP47(2−34) with microsomal membranes, and second, analyzed the structure of ICP47(2−34) in the membranelike bound state by NMR.

MATERIALS AND METHODS

Sample Preparation. ICP47(2−34) and peptides were synthesized by the solid-phase technique applying conventional Fmoc chemistry. Products were purified by preparative reversed-phase HPLC and their identity was verified by mass spectrometry. The initial NMR sample contained 4.3 mM ICP47(2−34) dissolved in 560 mM sodium dodecyl-d_{25} sulfate (SDS) in 90% H_2O/10% D_2O, pH 7.4. This sample was subsequently lyophilized and dissolved in 100% D_2O; the samples remained stable over several months at room temperature.

Preparation of Microsomes. Human TAP1 and TAP2 were coexpressed in Sf9 insect cells by using the baculovirus expression system as reported previously (*7*, *13*). TAP-containing microsomes were isolated by a combination of differential and sucrose density gradient centrifugation (*13*, *14*). The microsomal membranes were resuspended in phosphate-buffered saline with 1 mM 1,4-dithio-DL-threitol, snap-frozen in liquid nitrogen, and stored at −80 °C.

Peptide Transport Assay. TAP-containing microsomes (35 μg of total protein) were preincubated with 3 mM ATP in the absence or presence of 10 μM ICP47(2−34) in 100 μL of assay buffer [phosphate-buffered saline, 1 mM 1,4-dithio-DL-threitol, 5 mM $MgCl_2$, and 0.05% poly(ethylene glycol) 6000, pH 7.4] for 4 min at 37 °C before 250 nM radiolabeled reporter peptide RYWANATRST was added. After 4 min at 37 °C, peptide transport was stopped by adding 400 μL of ice-cold assay buffer and centrifugation (12000*g* for 8 min at 4 °C). After the pellets were washed with 500 μL of cold assay buffer, microsomes were lysed in 700 μL of NP-40 lysis buffer (50 mM Tris, 50 mM NaCl, 5 mM $MgCl_2$, and 1% NP-40, pH 7.4). N-Glycosylated and therefore translocated peptides were bound to 30 μL of concanavalin A−Sepharose (Sigma) while gently shaking for 1.5 h at 4 °C. After the beads were washed three times with 1 mL of lysis buffer, peptides were eluted with 200 mM methyl α-D-mannopyranoside and quantified by γ-counting. Background transport activity was measured in the presence of 3 mM ADP instead of ATP or a 400-fold molar excess of nonlabeled peptide. Peptides were radiolabeled with chloramine T-precoated glass vials purchased from Pierce. After a 20-min incubation of 7.5 nmol of reporter peptide and 0.5 mCi of $Na^{125}I$ in 250 μL of phosphate-buffered saline, pH 7.4, at room temperature, the iodinated peptide was removed and mixed with 250 μL of phosphate-buffered saline, pH 7.4, containing 10 mg/mL tyrosine and 2 mM NaI.

Peptide Binding and Competition Assays. TAP-containing microsomes were diluted with ice-cold assay buffer to a final protein concentration of 175 μg/mL. From this suspension, 150 μL was incubated with radiolabeled RRYNASTEL (310 nM) in the presence of various concentrations of ICP47(2−34). To reach equilibrium, samples were incubated for 45 min on ice. Subsequently, 350 μL of cold assay buffer was added and the microsomes were pelleted by centrifugation (12000*g* for 8 min at 4 °C). After the samples were washed with 500 μL of cold assay buffer, microsome-associated radioactivity was quantified by γ-counting. The amount of bound peptide was background-corrected for nonspecific binding in the presence of a 400-fold molar excess of nonlabeled peptide, which corresponds to 100% inhibition of peptide binding to TAP. To determine the dissociation constant (K_d) of ICP47(2−34), the inhibitor concentration was varied over 3 orders of magnitude and the data were fitted by a competition function as described (*14*).

Membrane Binding Assay. At room temperature, increasing amounts of radiolabeled ICP47(2−34) were incubated with microsomes from noninfected insect cells (100 μg of total protein) in 50 μL of assay buffer [phosphate-buffered saline, 1 mM 1,4-dithio-DL-threitol, 5 mM $MgCl_2$, and 0.05% poly(ethylene glycol) 6000, pH 7.4] for 15 min. After 400 μL of assay buffer was added, microsomes were pelleted by centrifugation (12000*g* for 8 min at 4 °C) and washed with 500 μL assay buffer. Membrane-associated ICP47(2−34) was quantified by γ-counting. ICP47(2−34) was synthesized and iodinated as described above.

NMR Experiments. Proton NMR spectra of ICP47(2−34) were acquired at 500, 600, and 750 MHz on the Bruker AMX-500, DRX-600, and DMX-750 spectrometers. Most data were collected at 307 K on the Bruker DRX-600 spectrometer. TOCSY and NOESY experiments were also repeated at 292 and 300 K on the DRX-750 and the AMX-500, respectively, for the sample in water. All two-dimensional spectra were collected with either 2048 or 4096 complex data points in $F2$, acquiring 256−400 increments in $F1$ for TOCSY and NOESY and 500−700 increments for COSY spectra. For the SDS/H_2O sample, the solvent signal was suppressed either by the pulsed field gradients with a 3−9−19 Watergate sequence (NOESY and TOCSY) or by low-power presaturation during the relaxation delay (COSY). To reduce the influence of spin diffusion and still have NOE intensities close to their maxima (*15*), the mixing time was 84 ms for the NOESY spectrum. The mixing times for TOCSY spectra were 56 and 58 ms. The D_2O TOCSY was acquired with a 62 ms clean MLEV-17 mixing sequence. The D_2O NOESY data were collected with a mixing time of 90 ms with presaturation of water. The baseline corrections were carried out on either side of the residual water signal. The data were processed with a Gaussian window function. No zero-filling was necessary. An amide proton exchange experiment was performed after lyophilization of ICP47(2−34)−SDS and dissolution of the complex in D_2O. A 2D NOESY spectrum was recorded within 2 h at 292 K and checked for the presence of cross-peaks that originate from H^N resonances.

Structure Calculations. A total of 40 structures were calculated by a previously described procedure (*16*) using a simulated annealing protocol implemented in the program X-PLOR (*17*). Distance constraints were collected from 2D NOESY spectra in H_2O and D_2O and classified according to the peak intensities as very strong (2.0−2.6 Å), strong (2.3−3.1 Å), medium (2.8−3.5 Å), weak-medium (3.6−4.2 Å), or weak (4.2−5.0 Å). All protons were explicitly defined in the structure calculations; in some cases, however, additional terms were added to the upper bounds that correspond to the pseudoatom correction introduced by Wüthrich (*18*). A total of 93 interresidue $^1H-^1H$ distances have been used in the calculations.

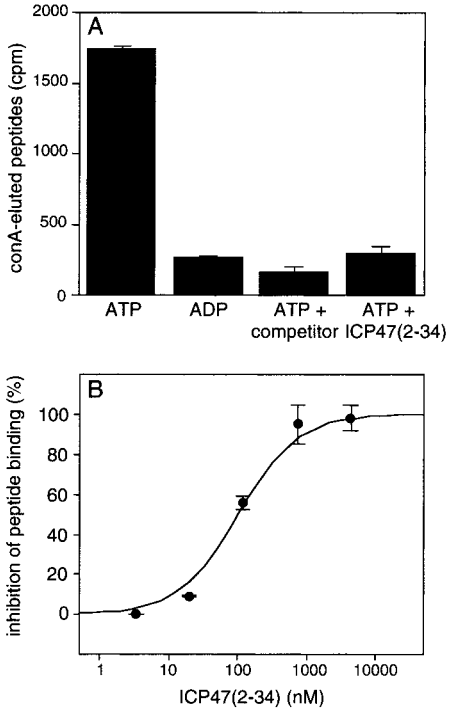

FIGURE 1: ICP47(2−34) blocks TAP-dependent peptide transport and peptide binding to TAP. (A) Peptide transport into TAP-containing insect microsomes was measured for 4 min at 37 °C in the presence or absence of 10 μM ICP47(2−34). *In vitro* transport assays were performed with 250 nM radiolabeled reporter peptide RYWANATRST and 3 mM ATP. N-Glycosylated and therefore translocated peptides were quantified by γ-counting after binding to and specific elution from concanavalin A−Sepharose. Nonspecific transport was determined in the presence of 3 mM ADP or a 400-fold molar excess of the nonlabeled peptide. (B) Peptide binding to the TAP complex was analyzed in the presence of various concentrations of ICP47(2−34). TAP-containing microsomes were incubated with 310 nM radiolabeled reporter peptide RRYNASTEL for 45 min on ice. Background binding was determined by using a 400-fold molar excess of nonlabeled peptide. By fitting of the data (*14*), an IC_{50} of 100 ± 14 nM was calculated.

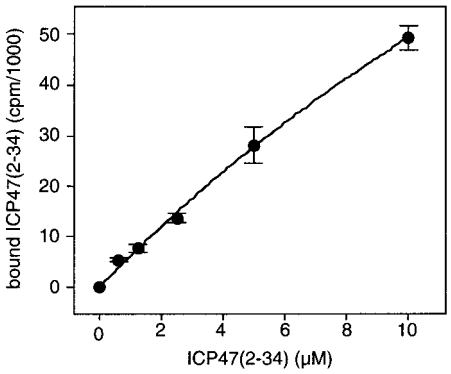

FIGURE 2: ICP47(2−34) binds to microsomes. Microsomes prepared from noninfected insect cells were incubated with various concentrations of radiolabeled ICP47(2−34) for 15 min at room temperature. After the microsomes were washed, membrane adsorption of ICP47(2−34) was quantified by γ-counting. The affinity constant for binding to microsomal membranes was determined to be K_d = 34 ± 9 μM assuming a Langmuir-type adsorption.

RESULTS

ICP47(2−34) Blocks Peptide Binding to and Peptide Transport by TAP. The activity of the synthetic ICP47(2−34) was analyzed by an *in vitro* peptide transport assay based on specific N-glycosylation in microsomes. As shown in Figure 1A, ICP47(2−34) completely blocks TAP-specific peptide translocation of radiolabeled reporter peptides into microsomes. Moreover, we quantified the binding affinity of ICP47(2−34) to TAP and its ability to inhibit peptide binding by competition assays (Figure 1B). An affinity binding constant of K_d = 100 ± 14 nM was determined, which is in good agreement with the affinity constant for the full-length ICP47 (*7*, *8*). In summary, fragment ICP47-(2−34) shows all characteristics of wild-type ICP47 and therefore it is an ideal model to investigate the structure of this unique inhibitor of the TAP transport complex.

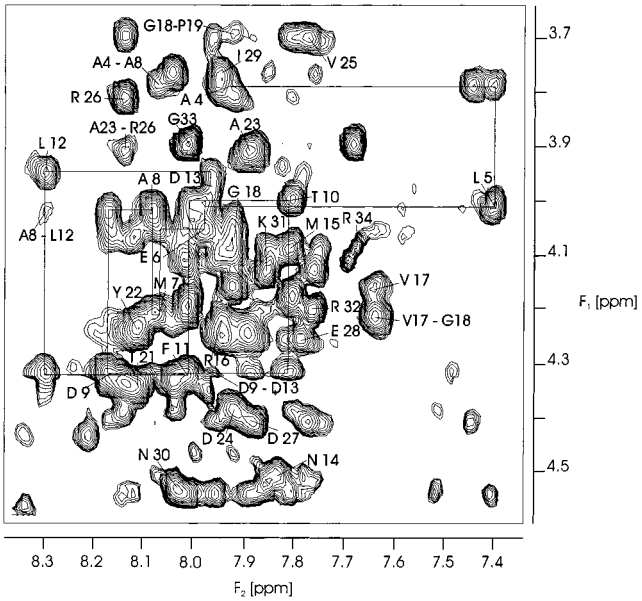

FIGURE 3: NOESY spectrum (307 K) of the H^N (F_2 axis)−H^α (F_1 axis) region of ICP47(2−34) associated with SDS micelles. The intraresidue H^N−H^α cross-peaks are marked by one-letter amino acid symbols. The lines indicate the assignment pathway for residues 4−13.

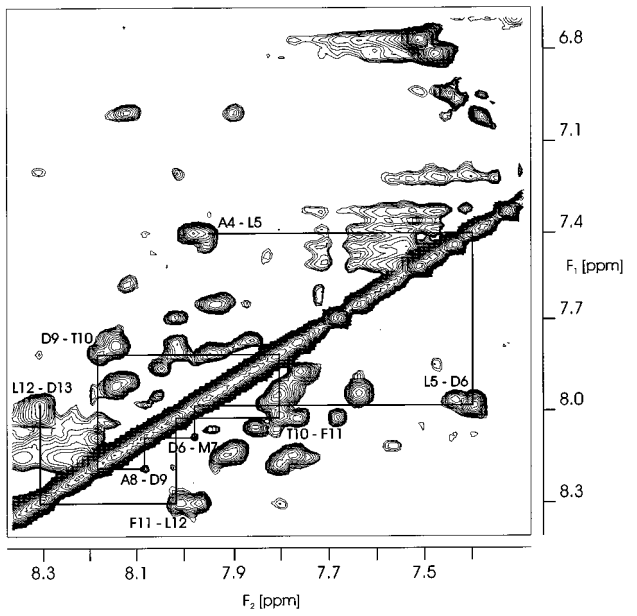

FIGURE 4: NOESY spectrum (307 K) of the H^N (F_2 axis)−H^N (F_1 axis) region of ICP47(2−34) associated with SDS micelles. An example of the assignments of the H^N−H^N connectivities is shown for residues 4−13.

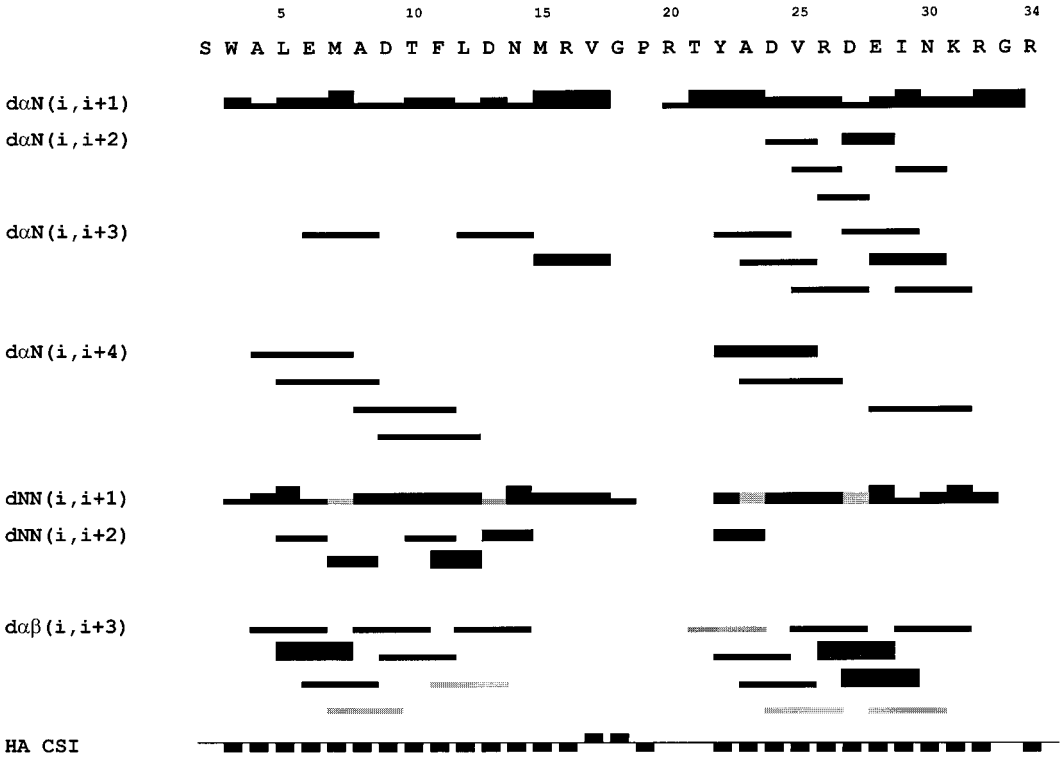

FIGURE 5: Summary of sequential and medium range ($|i - j| < 5$) connectivities involving H^N, H^α, and H^β protons. The $d_{NN}(i, i + 1)$ and $d_{\alpha\beta}(i, i + 3)$ connectivities shown in gray could not be established because of the spectral overlap. The H^δ(Pro19)−H^N(Gly18) NOE is shown along the same line as the H^N−H^N connectivities. The NOE intensities, classified as weak, medium, and strong, are represented by the heights of bars. The chemical shift index (HA CSI) is given below the sequence with negative bars indicating α-helical regions.

Interaction with Microsomes. It has recently been shown that the membranes or membrane mimetics induces an α-helical structure of ICP47, suggesting that the viral TAP inhibitor binds to membranes (*12*). Because a direct physical interaction of ICP47 with microsomes lacking TAP complexes has not been demonstrated so far, the binding of ICP47 to microsomal membranes was investigated. Microsomes prepared from noninfected insect cells were incubated with an increasing amount of radiolabeled ICP47-(2−34) and washed, and the membrane-associated inhibitor was quantified. As shown in Figure 2 the polypeptide binds in a dose-dependent manner to microsomes, revealing an affinity constant $K_d = 34 \pm 9$ μM. ICP47(2−34) shows a 350−400 times weaker affinity to microsomal membranes without than with human TAP. We avoided full saturation in order to circumvent secondary effects such as potential membrane disruptions or aggregation of ICP47 at high concentrations. Although the dissociation rate was not specifically examined in this set of assays, ICP47(2−34) remained bound even after extensive washing, indicating a stable ICP47−membrane interaction. Additionally, the membrane association explains the biphasic binding characteristics of ICP47 to TAP-containing microsomes (data not shown). Consequently, it is likely that the high affinity of ICP47 for TAP is based partially on the preenrichment at the ER membrane. Therefore, the investigation of the membrane-bound structure of the viral inhibitor represents an important contribution to the understanding of ICP47 function.

NMR Resonance Assignments. A sequence-specific resonance assignment (*16*) was carried out starting with spectra taken at 307 K. The spectra at 292 and 300 K were assigned after the assignment of the high-temperature spectrum was achieved. The positions of the peaks were nearly identical at all three temperatures, but line broadening at lower temperatures obscured many cross-peaks of the anticipated helices. The amino acid spin systems were identified by analysis of the TOCSY spectrum at 307 K. The TOCSY spectra at lower temperatures could not be used because of their poor quality. The 292 K NOESY spectrum provided useful information for assignment of several amino acids, for example Trp-3, which could not be directly assigned in the spectra at 307 K. Figure 3 shows the fingerprint region of the 307 K NOESY spectrum and indicates the sequential assignment for the helix between residues 4 and 15. Figure 4 shows the H^N−H^N region of the same NOESY spectrum. The list of the assignments at this temperature is given in Table S1 of the Supporting Information.

Secondary Structure. A summary of the NOEs that are diagnostic for the secondary structure is given in Figure 5. The NMR spectra of ICP47(2−34) showed lack of long-range NOEs (between amino acids further apart than 4 residues). The evidence for ordered conformations in peptides consists of patterns of NOE connectivities that was discussed in detail by Dyson et al. (*19*, *20*). From these NOEs it also is frequently possible to qualitatively assess the populations of different types of secondary structure conformations (*19*−*21*). An extended conformation shows very strong $d_{\alpha N}(i, i + 1)$ NOEs and no H^N−H^N intensities for each pair of residues. This is in contrast to the α-conformation, for which a strong $d_{NN}(i, i + 1)$ NOE for a pair of residues is accompanied by a weak $d_{\alpha N}(i, i + 1)$ intensity. The average NOE is a mixture of extended and α-conformations. For any pair of residues, strong NOEs of each state will contribute to the average NOE over these two discrete states. The presence of the strong H^N−H^N and H^N−H^α connectivities thus indicates that a population of the peptide occupies both

the β- and α-regions of the (ϕ, ψ) space. It is clear that $d_{\alpha N}(i, i+1)$ connectivities cannot be used for characterization of helices and turns in peptides since the unfolded conformers give rise to strong $d_{\alpha N}(i, i+1)$ NOEs, thus obscuring the NOE originating from turns that contain weak $d_{\alpha N}(i, i+1)$. Turns and loose helical structures can, however, be detected via the presence of several medium range interactions: $H^N(i)-H^N(i+2)$, $H^\alpha(i)-H^N(i+3)$, $H^\alpha(i)-N^H(i+4)$, and $H^\alpha(i)-H^\beta(i+3)$ connectivities. The NOESY spectra of ICP47(2−34) showed the presence of the $H^N(i)-H^N(i+1)$, $H^N(i)-H^N(i+2)$, $H^\alpha(i)-H^N(i+3)$, $H^\alpha(i)-N^H(i+4)$, and $H^\alpha(i)-H^\beta(i+3)$ connectivities for residues from 4 to 15 (Figure 4). These are characteristic for an α-helical conformation. We could not detect any turnlike structures between residues 11−15 in ICP47(2−34), although we looked for the turn-diagnostic NOEs especially carefully. The segment from residues 22 to 32 showed the α-helical H^N-H^N, $H^\alpha(i)-H^N(i+1)$, $H^\alpha(i)-H^N(i+3)$, and $H^\alpha(i)-H^\beta(i+3)$ interactions. Further support for helical regions between residues 4−15 and 22−32 was provided by the amide exchange data (*18*). Slowly exchanging amides were observed in the central residues of the helical segments (residues 8−12 and 24−30). In addition, the proton resonances for residues 4−16 and 21−34 were shifted upfield relative to random coil positions in the ICP47(2−34) peptide spectra (Figure 3) by 0.2−0.6 ppm, which is characteristic of helical structures (*22*, *23*). The coupling constant data could not be used for the secondary structure determination because of broad lines in the SDS solutions. Figure 6 shows the relative helicity of the peptide. The ratio R of the intensities I of $d_{NN}(i, i+1)$ and $d_{\alpha N}(i, i+1)$ NOEs at each position is given in Figure 6A (*24*):

$$R = [I(H^N_i, H^N_{i+1})]/[I(H^\alpha_i, H^N_{i+1})]$$

The values for the ICP47(2−34) peptide are above 1.0 in parts of the peptide, indicating a substantial population of conformations in the α-region of (ϕ, ψ) space. However, the relative intensities of the sequential NOEs alone are quite inaccurate since the $d_{NN}(i, i+1)$ and $d_{\alpha N}(i, i+1)$ NOEs reflect the population of the folded and unfolded conformers. As pointed out by Waltho et al. (*22*) relative intensities of the $d_{\alpha\beta}(i, i+3)$ NOEs can provide also valuable insights into the relative helical populations. The intensities of the $H^\alpha(i)-H^N(i+3)$ connectivities (scaled for the number of protons involved) are plotted against the residue number in Figure 6B and indicate again high populations of α-helical structures for residues 4−15 and 22−32. We have therefore decided to convert the NOE data into distance constraints in order to calculate the structure of ICP47(2−34) from these NMR data. A total of 40 structures were calculated by the simulated annealing method with the program XPLOR 3.1 (*17*). Thirty from these 40 structures satisfy the experimental constraints with small deviations from idealized covalent geometry. The structure calculation shows that the conformation of the peptide bound to SDS consists of two major helices extending from residues 4 to 15 and from 22 to 32 (Figure 7). The two helices are very well defined in terms of both average atomic rms differences (ca. 0.37 Å) and backbone torsion angles (less than 30°). There are no distance constraints violations larger than 0.5 Å and the structures display low total energies (Table S2, Supporting Information).

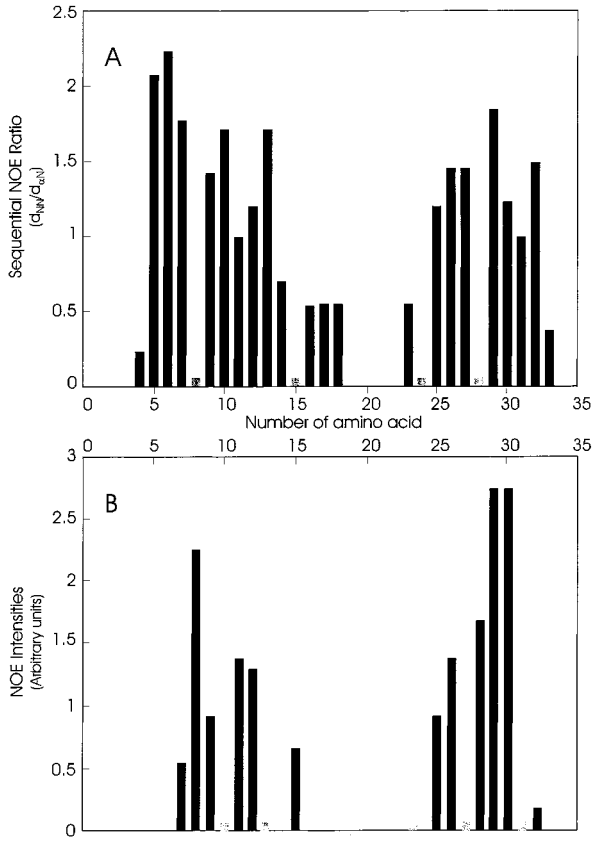

FIGURE 6: (A) Ratio of the intensities of the sequential $d_{NN}(i, i+1)/d_{\alpha N}(i, i+1)$ NOEs, calculated from the height of the peaks obtained from the NOESY spectrum of Figures 3 and 4, plotted against residue number. (B) Intensities of the $d_{\alpha\beta}(i, i+3)$ NOE connectivities plotted against the number of residues, scaled according to the number of equivalent protons contributed to the NOE. Gray bars indicate lack of data due to spectral overlap.

In contrast to the well-defined helices, the loop consisting of amino acids 16−21 displays high variability and the N- and C-terminal regions of the peptide between residues 2 and 3 and between 32 and 34, respectively, adopt entirely disordered conformations.

DISCUSSION

The herpes simplex virus protein ICP47 represents an interesting molecule due to its ability to block the antigen presentation by inhibition of TAP function. Most strikingly, a polypeptide of only 32 amino acid residues in length, ICP47(3−34), retains full activity to block TAP function (*11*). By circular dichroism analysis, ICP47 was found to be mostly unstructured in aqueous solution. However, in the presence of membranes or lipidlike solvents such as TFE/water or SDS/water mixtures, an α-helical conformation is induced, implying that ICP47 interacts with membranes (*12*). By use of Trp-3 as an environment-sensitive probe, evidence for ICP47−membrane interaction was obtained by fluorescence spectroscopy (*12*).

In this report, the specific association of ICP47 with microsomal membranes and the structure of the membrane-bound state has been investigated. For these studies, we used ICP47(2−34) that was synthesized by solid-phase synthesis. In the first set of experiments, we could demonstrate that ICP47(2−34) has the same activity as the wild-type protein with respect to blocking peptide binding to and transport via

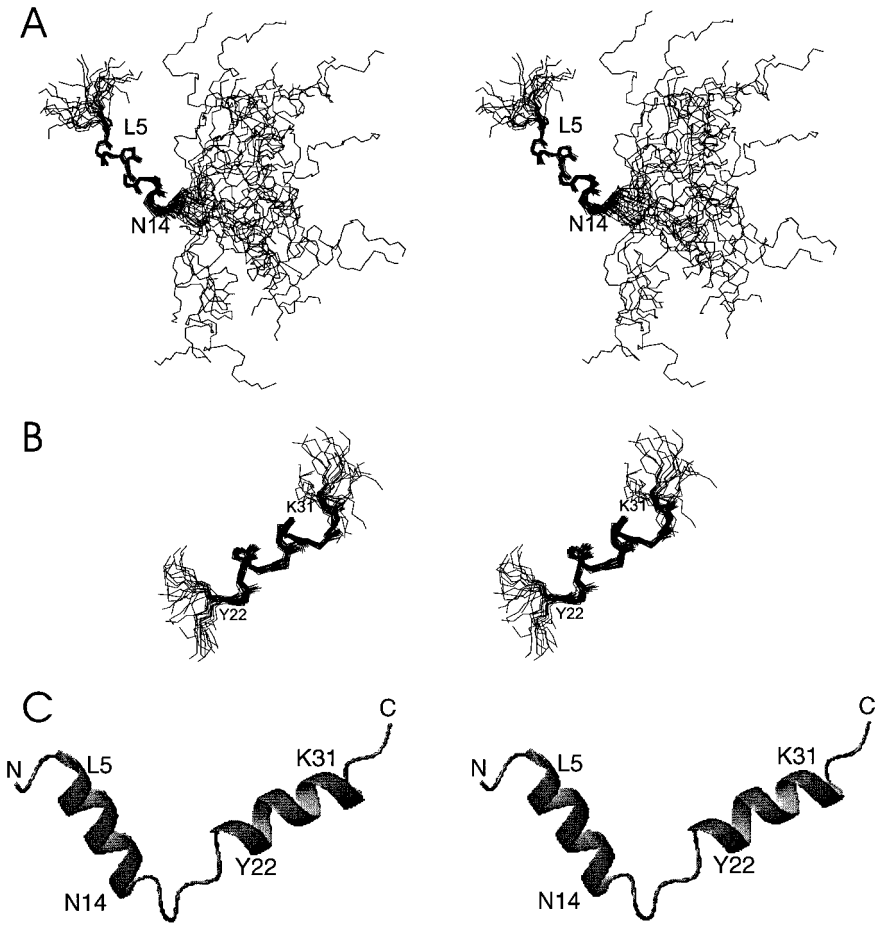

FIGURE 7: Backbone stereoview of the SDS-associated ICP47(2−34) structures. (A) Superposition of 20 structures (residues 2−30) best fitted to residues 5−16. (B) Superposition of backbone atoms (residues 21−33) best fitted to residues 22−31. (C) Ribbon drawing of a single structure of ICP47(2−34) bound to SDS micelles.

TAP. ICP47(2−34) therefore represents an ideal model to investigate the structure and function of ICP47. In the second set of experiments, we could show that ICP47(2−34) binds to membranes even in the absence of TAP. The amount of membrane-bound ICP47 is concentration-dependent. Membrane binding follows a Langmuir-type adsorption with an affinity constant of $K_d = 34 \pm 9\ \mu$M. Although the ICP47−membrane interaction is approximately 300-fold weaker than the association with human TAP, the membrane adsorption could be a prerequisite for high-affinity binding of ICP47 to TAP by increasing the local concentration of ICP47 or by inducing a conformation optimal for binding to TAP. It is interesting to note that P-glycoprotein (multidrug resistance protein, MDR1), which is a close TAP homologue, takes up substrates from the membrane. In analogy, the understanding of the membrane adsorption process and a detailed knowledge of the membrane-induced conformational changes appear to be important in disclosing the structural and mechanistic aspects of TAP inhibition by ICP47. Therefore, we analyzed the structure of ICP47 by NMR techniques. Due to the intrinsic difficulties in NMR analysis of proteins in the membrane-bound state, NMR studies of ICP47(2−34) were performed in micellar solution with deuterated SDS. It was previously shown that this membrane mimetic induces a similar conformational change as binding to membranes does (*12*). The NMR analysis of ICP47(2−34) was performed in a 130-fold molar excess of SDS. Assuming that 60−70 molecules form one micelle under these conditions, the solution should contain an excess of 2 micelles per ICP47 molecule. The NMR data and physical characteristics of the sample (i.e., nongelling after several weeks) suggest that there is a strong association of ICP47(2−34) with SDS micelles and that the NMR structure reflects the micelle-bound state. This structure comprises mostly helical conformation for the peptide that is only broken by a loop between Val-17 and Thr-21. The N-terminal α-helix 4−15/16 matches the predicted α-helix covering positions 3−13 (*11*, *12*), whereas the second α-helix 21/22−32 was only predicted with lower significance. The relevance of the N-terminal α-helix is underlined by nonactive ICP47 mutants bearing a proline at position 19, which is known to break α-helices (*11*). No contact between both α-helices could be detected, allowing an independent movement of both α-helical regions. Although it cannot be extracted from our data directly that the membrane-bound structure represents the TAP-bound conformation, due to the high affinity of ICP47 for TAP the energetically unfavorable melting of an α-helix causing a high activation barrier appears to be unlikely. Hence, one can speculate that the helix−turn−helix motif might be a prerequisite for the binding of one α-helix to TAP while the other α-helix remains associated with the membrane. Alternatively, this structural flexibility may be required in order not to hinder the transformation from a lose to a tight TAP conformation followed by the binding of ICP47 to TAP as suggested by Lacaille et al. (*9*).

The helix−turn−helix motif of ICP47(2−34) is similar to those found in many integral membrane proteins, for example, the major coat proteins of filamentous bacteriophage (*25*−*30*), and to the antibacterial and lytic polypeptides such as, for example, cecropins (*31*, *32*). The secondary structures of both of these groups of peptides in membrane-like solvents consist of two helical regions. In the major coat proteins, the helices are well-defined and stable, with the N-terminal amphipathic helix of 9−22 residues and the C-terminal hydrophobic helix of 17−19 residues. The N-terminal helix lies at the membrane interface and is perpendicular to the C-terminal helix, which spans the micelle (*26*−*31*). In ICP47(2−34) both helices are amphipathic and are shorter. The topology of secondary structure of ICP47(2−34) is therefore more similar to that of cecropin, which has two amphipathic helices of 12−15 residues long (*31*). The biological activity of cecropins is best explained by a carpetlike mechanism of their interaction with the lipid membrane. In this model cecropin adopts an orientation parallel to the membrane surface and does not insert itself into bilayer (*32*). Our present study on ICP47(2−34) also supports such a mode of interaction and thus confirms our previously proposed model in which the bound ICP47(2−34) is at the surface of the membrane and does not make a transmembrane entry (*12*).

In summary, we confirm and extend the TAP inhibition model proposed by Beinert et al. (*12*). The adsorption of ICP47 to the ER membrane is the first and initial step of blocking TAP function, thereby generating a high local ICP47 concentration and forming a defined structure. This membrane-induced conformational change prepares the ICP47 molecule for the interaction with TAP by arranging the essential side chains in an optimal orientation. In the second step ICP47 binds to TAP and finally blocks the peptide binding site.

CONCLUSION

In the current study, the structure of the active domain of ICP47 has been determined in the presence of SDS micelles. Given that the SDS concentration was more than 100-fold higher than that of ICP47(2−34) and that there are 60−70 molecules per micelle, the solution contains an excess of micelles over the ICP47(2−34) molecules. The NMR data and physical characteristics of the sample (i.e., nongelling after several weeks) suggest that there is a strong association of ICP47(2−34) with SDS micelles and that the structure here reflect a micelle-bound state. This structure comprises a mostly amphipathic helical conformation for the peptide that is only broken by a loop between Val-17 and Thr-21.

ACKNOWLEDGMENT

We thank Drs. Lutz Schmitt and Rupert Abele for critical reading and helpful discussion.

SUPPORTING INFORMATION AVAILABLE

Table S1, with the ^{1}H chemical shifts of ICP47(2−34)-SDS; the list of distance constraints; and Table S2, with parameters that characterize the structure determination. This material is available free of charge via the Internet at http://pubs.acs.org.

REFERENCES

1. Pamer, E., and Cresswell, P. (1998) *Annu. Rev. Immunol. 16*, 323−358.
2. Ploegh, H. L. (1998) *Science 280*, 248−253.
3. York, I. A., Roop, C., Andrews, D. W., Riddell, S. R., Graham, F. L., and Johnson, D. C. (1994) *Cell 77*, 525−535.
4. Hill, A. B., Barnett, B. C., McMichael, A. J., and McGeoch, D. J. (1994) *J. Immunol. 152*, 2736−2741.
5. Hill, A., Jugovic, P., York, I., Russ, G., Bennink, J., Yewdell, J., Ploegh, H., and Johnson, D. (1995) *Nature 375*, 411−415.
6. Früh, K., Ahn, K., Djaballah, H., Sempé, P., van Endert, P. M., Tampé, R., Peterson, P. A., and Yang, Y. (1995) *Nature 375*, 415−418.
7. Ahn, K., Meyer, T. H., Uebel, S., Sempé, P., Djaballah, H., Yang, Y., Peterson, P. A., Früh, K., and Tampé, R. (1996) *EMBO J. 15*, 3247−3255.
8. Tomazin, R., Hill, A. B., Jugovic, P., York, I., van Endert, P., Ploegh, H. L., Andrews, D. W., and Johnson, D. C. (1996) *EMBO J. 15*, 3256−3266.
9. Lacaille, V. G., and Androlewicz, M. J. (1998) *J. Biol. Chem. 273*, 17386-17390.
10. Galocha, B., Hill, A., Barnett, B. C., Dolan, A., Raimondi, A., Cook, R. F., Brunner, J., Mcgeoch, D. J., and Ploegh, H. L. (1997) *J. Exp. Med. 185*, 1565−1572.
11. Neumann, L., Kraas, W., Uebel, S., Jung, G., and Tampe, R. (1997) *J. Mol. Biol. 272*, 484−492.
12. Beinert, D., Neumann, L., Uebel, S., and Tampé, R. (1997) *Biochemistry 36*, 4694−4700.
13. Meyer, T. H., van Endert, P. M., Uebel, S., Ehring, B., and Tampé, R. (1994) *FEBS Lett. 351*, 443−447.
14. Uebel, S., Meyer, T. H., Kraas, W., Kienle, S., Jung, G., Wiesmüller, K. H., and Tampé, R. (1995) *J. Biol. Chem. 270*, 18512−18516.
15. Neuhaus, D., and Williamson, M. (1989) *The nuclear Overhauser effect in structural and conformational analysis*, VCH Publishers, New York.
16. Holak, T. A., Gondol, D., Otlewski, J., and Wilusz, T. (1989). *J. Mol. Biol. 210*, 635−648.
17. Brünger, A. T. (1993) XPLOR Version 3.1 Manual, Yale University, New Haven, CT.
18. Wüthrich, K. (1986) *NMR of proteins and nucleic acids*, John Wiley & Sons, Inc., New York.
19. Dyson, H. J., Rance, M., Houghten, R. A., Wright, P. E., and Lerner, R. A. (1988) *J. Mol. Biol. 201*, 201−217.
20. Dyson, H. J., Rance, M., Houghten, R. A., Lerner, R. A., and Wright, P. E. (1988) *J. Mol. Biol. 201*, 161−200.
21. Bruch, M. D., McKnight, C. J., and Gierasch, L. M. (1989) *Biochemistry 28*, 8554−8561.
22. Waltho, J. P., Feher, V. A., Merutka, G., Dyson, H. J., and Wright, P. E. (1993) *Biochemistry 32*, 6337−6347.
23. Bundi, A., and Wüthrich, K. (1979) *Biopolymers 18*, 285−312.
24. Wishart, D. S., Sykes, B. D., and Richards, F. M. (1992) *Biochemistry 31*, 1647−1651.
25. Opella, S. J. (1997) *Nat. Struct. Biol. 4*(Suppl.), 845−848.
26. McDonnell, P. A., Shon, K., Kim, Y., and Opella, S. J. (1993) *J. Mol. Biol. 233*, 447−463.
27. Almeida, F. C., and Opella, S. J. (1997) *J. Mol. Biol. 270*, 481−495.
28. Henry, G. D., and Sykes, B. D. (1992) *Biochemistry 31*, 5284−5297.
29. van de Ven, F. J., van Os, J. W., Aelen, J. M., Wymenga, S. S., Remerowski, M. L., Konings, R. N., and Hilbers, C. W. (1993) *Biochemistry 32*, 8322−8328.
30. Williams, K. A., Farrow, N. A., Deber, C. M., and Kay, L. E. (1996) *Biochemistry 35*, 5145−5157.
31. Holak, T. A., Engstrom, A., Kraulis, P. J., Lindeberg, G., Bennich, H., Jones, T. A., Gronenborn, A. M., and Clore, G. M. (1988) *Biochemistry 27*, 7620−7629.
32. Gazit, E., Miller, I. R., Biggin, P. C., Sansom, M. S., and Shai, Y. (1996) *J. Mol. Biol. 258*, 860−870.

BI9909647